ACS APPLIED MATERIALS & INTERFACES

Research Article

www.acsami.org

Engineering of Surface Chemistry for Enhanced Sensitivity in Nanoporous Interferometric Sensing Platforms

Cheryl Suwen Law,[†,§] Georgina M. Sylvia,[‡,§,∥] Madieh Nemati,[†] Jingxian Yu,[‡,§,∥] Dusan Losic,[†] Andrew D. Abell,*[,‡,§,∥] and Abel Santos*[,†,‡,§]

[†]School of Chemical Engineering, [‡]Department of Chemistry, [§]Institute for Photonics and Advanced Sensing (IPAS), and [∥]ARC Centre of Excellence for Nanoscale BioPhotonics (CNBP), The University of Adelaide, Adelaide, SA 5005, Australia

Supporting Information

ABSTRACT: We explore new approaches to engineering the surface chemistry of interferometric sensing platforms based on nanoporous anodic alumina (NAA) and reflectometric interference spectroscopy (RIfS). Two surface engineering strategies are presented, namely (i) selective chemical functionalization of the inner surface of NAA pores with amine-terminated thiol molecules and (ii) selective chemical functionalization of the top surface of NAA with dithiol molecules. The strong molecular interaction of Au^{3+} ions with thiol-containing functional molecules of alkane chain or peptide character provides a model sensing system with which to assess the sensitivity of these NAA platforms by both molecular feature and surface engineering. Changes in the effective optical thickness of the functionalized NAA photonic films (i.e., sensing principle), in response to gold ions, are monitored in real-time by RIfS. 6-Amino-1-hexanethiol (inner surface) and 1,6-hexanedithiol (top surface), the most sensitive functional molecules from approaches i and ii, respectively, were combined into a third sensing strategy whereby the NAA platforms are functionalized on both the top and inner surfaces concurrently. Engineering of the surface according to this approach resulted in an additive enhancement in sensitivity of up to 5-fold compared to previously reported systems. This study advances the rational engineering of surface chemistry for interferometric sensing on nanoporous platforms with potential applications for real-time monitoring of multiple analytes in dynamic environments.

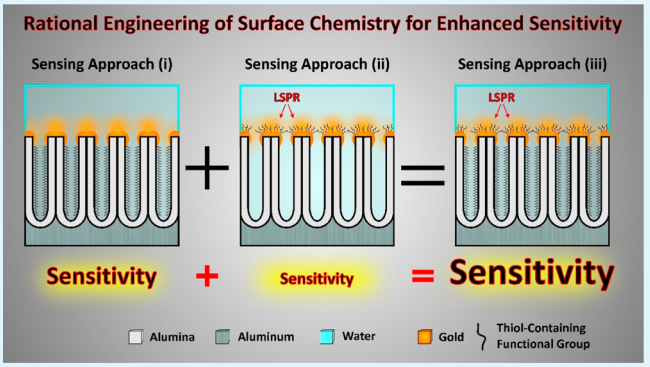

KEYWORDS: *nanoporous anodic alumina, reflectometric interference spectroscopy, surface chemistry engineering, optical sensing, sensing performance*

1. INTRODUCTION

Optical sensors are powerful analytical tools that play vital roles in biomedical research, environmental monitoring, homeland security, and other applications.[1] Advantages of optical sensing systems include immunity to electromagnetic interference, label-free and remote sensing capabilities, and identification of analytes of interest by characteristic spectroscopic signatures.[2,3] Optical sensors collect analytical information through the interaction between light and matter using optical transduction techniques such as surface plasmon resonance (SPR), surface-enhanced Raman scattering (SERS), photoluminescence, and interferometry.[4−7] Among these, interferometric sensors offer a versatile, label-free sensing approach for broad sensing applications.[8−15] The underlying principle of reflectometric interference spectroscopy (RIfS) is based on white light interferometry on solid thin films, which results in the formation of a characteristic interference pattern by the Fabry−Pérot effect.[8,9] Pioneering RIfS systems combined functional polymeric thin films deposited onto glass slides as sensing platforms for gas sensing,[8,10] label-free immunosensing,[10] and biomolecular interaction analysis (BIA).[9,11] The use of nanoporous thin films based on porous silicon as transducer elements opened new opportunities to develop advanced sensing systems for the detection of small organic molecules, DNA, and proteins.[12−15] The nanoporous structure of porous silicon makes it an excellent platform for the development of photonic structures with precisely engineered optical properties such as well-resolved Fabry−Pérot fringes in the RIfS spectrum. Nevertheless, the relatively poor chemical stability in aqueous media of porous silicon leads to unstable optical signals, which is undesirable for practical sensing applications.[16,17] Alternative nanoporous materials, such as nanoporous anodic alumina (NAA), demonstrate similar advantages to those of porous silicon while addressing chemical instability limitations due to the inert nature of alumina (aluminum oxide, Al_2O_3). Versatility of nanopore geometry and surface chemistry, chemical and mechanical stability, and optical properties make NAA an excellent platform for developing interferometric sensing

Received: January 22, 2017
Accepted: February 27, 2017
Published: February 27, 2017

DOI: 10.1021/acsami.7b01116
ACS Appl. Mater. Interfaces XXXX, XXX, XXX−XXX

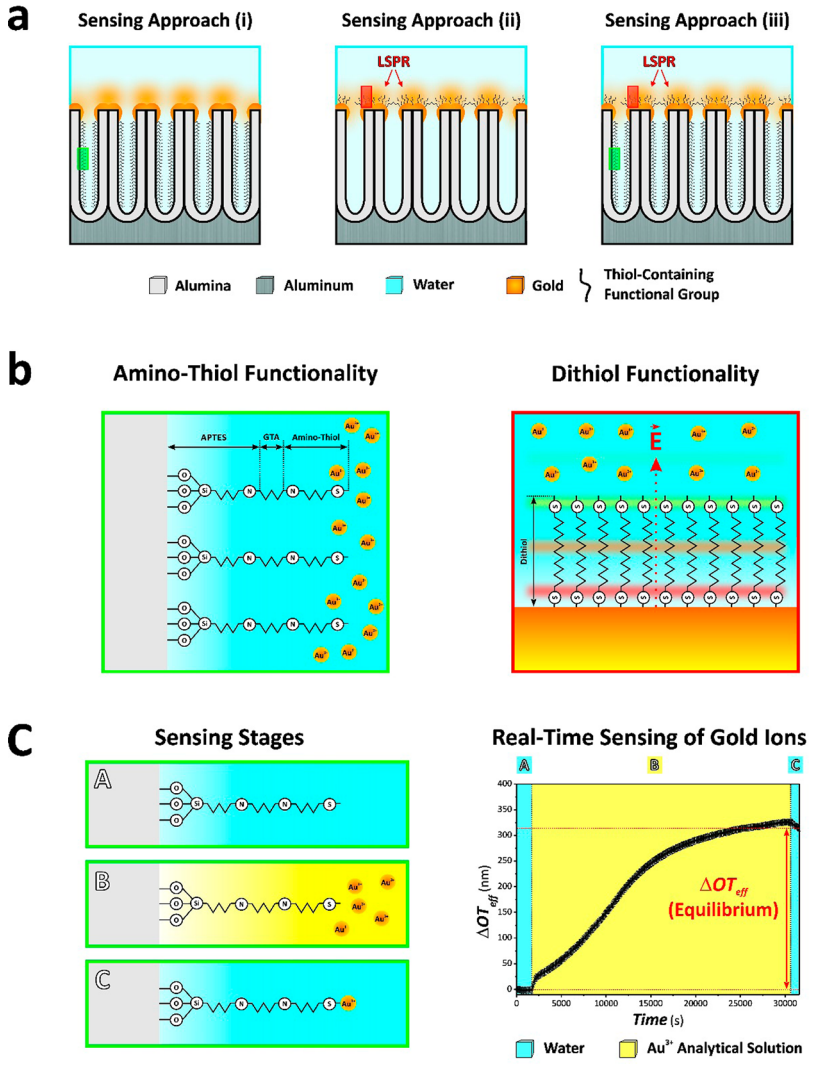

Figure 1. Sensing concepts and surface chemistries of NAA sensing platforms in combination with RIfS. (a) Sensing approaches used in our study: (i) selective functionalization with amino-thiol functional molecules inside the nanopores of NAA platforms, (ii) selective functionalization with dithiol functional molecules on the top surface of NAA platforms, and (iii) selective dual functionalization with amino-thiol and dithiol functional molecules inside the nanopores and on the top surface of NAA platforms, respectively. (b) Details of the surface chemistry structure for amino-thiol (left: magnified view of green rectangle shown in (a)) and dithiol (right: magnified view of red rectangle shown in (b)) functional molecules (note: for dithiol molecules, a localized surface plasmon resonance (LSPR) sensing approach was used, where the sensitivity of the system relies on the electromagnetic field generated in gold-coated NAA platforms, $\vec{E}$). (c) Stages of the sensing approach used in our study (left) and example of real-time sensing of gold ions in NAA platforms based on changes in the effective optical thickness measured by RIfS (note: real sensing for 8-amino-1-octanethiol for $[Au^{3+}] = 80\ \mu M$).

devices.[18] The combination of RIfS with NAA platforms has recently shown significant and promising potential for qualitative and quantitative detection of a broad range of analytes, such as gases, metal ions, biomolecules, and organic molecules.[19−25]

The sensitivity of interferometric sensors based on NAA and analogous nanoporous materials relies on the magnitude of the interaction between the nanoporous matrix and analyte molecules.[26,27] This interaction is translated into changes in the effective medium of the nanoporous film, the magnitude of which is established by five main factors, including (i) the optical properties of the analyte molecules, (ii) the size of the analyte molecules, (iii) the nature of the medium filling the nanopores (e.g., air or water), (iv) the chemical and physical interaction between the analyte molecules and the surface of the nanoporous matrix, and (v) the effective medium of the sensing platform.[25] The surface of NAA can be chemically modified with different functional molecules in order to attain chemical selectivity toward analytes of interest.[25] This factor is of critical importance, not only to selectively capture targeted analyte molecules but also for the sensitivity of the system, as this is strongly dependent on how surface functional groups interact with analyte molecules. Therefore, a suitable chemical functionalization strategy can result in enhanced sensing performances, which is a critical aspect to consider in the development of optical sensing systems for real-time monitoring of analytes in dynamic environments.

Herein, we demonstrate that a rational engineering of the surface chemistry in NAA interferometric platforms can significantly enhance the overall sensing performance. In this study, the gold−thiol interaction in NAA interferometric platforms was chosen as a sensing binding model to discern the effect of different factors upon the overall sensitivity. NAA platforms were functionalized with different thiol-containing

DOI: 10.1021/acsami.7b01116
ACS Appl. Mater. Interfaces XXXX, XXX, XXX−XXX

Table 1. Summary of the Characteristics of the Different Functional Molecules Used in Our Study

Functional Molecule Name	Functional Molecule Structure	Molecular Parameter	Sensing Approach	Molecular Mass (g mol^{-1})	Contact Angle (^{0})
L-cysteine	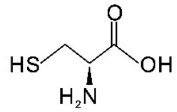			121.16	36 ± 2
Cysteamine	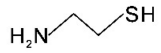			113.61	39 ± 3
L-cysteine Methyl Ester	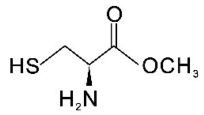	Functional Features	(i)	171.65	50 ± 2
AAC	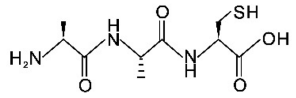			263.42	59 ± 3
3-amino-1-propanethiol				127.64	34 ± 2
6-amino-1-hexanethiol	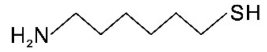	Molecular Length	(i)	169.72	51 ± 3
8-amino-1-octanethiol	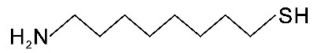			197.77	65 ± 2
1,3-propanedithiol				108.23	105 ± 2
1,6-hexanedithiol	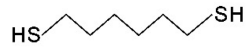	Molecular Length	(ii)	150.31	113 ± 1
1,9-nonanedithiol	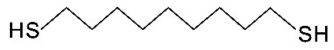			192.39	120 ± 5

functional molecules. Three sensing approaches were used to establish the effect of these functional configurations on the sensing performance (Figure 1a). This involved (i) selective chemical functionalization of the inner surface of NAA with amino-thiol molecules of different molecular features and sizes, (ii) selective chemical functionalization of the top surface of NAA with dithiol molecules of different sizes, and (iii) selective chemical functionalization of both the top and inner surface of NAA with amino-thiol molecules and dithiol molecules. Changes in the effective optical thickness of NAA platforms after exposure to analytical solutions containing gold ions (Au^{3+}) are used as the sensing principle (Figure 1b). This process is monitored in real time by RIfS, enabling the real-time assessment of the interaction between thiol functional groups present in NAA platforms and Au^{3+} ions (Figure 1c).

2. EXPERIMENTAL SECTION

2.1. Materials. High purity (99.9997%) aluminum (Al) foils 0.32 mm thick were supplied by Goodfellow Cambridge Ltd. (UK). Oxalic acid ($H_2C_2O_4$), perchloric acid ($HClO_4$), chromium trioxide (CrO_3), 3-aminotrimethoxysilane ($H_2N(CH_2)_3Si(OC_2H_5)_3$, APTES), hydrogen peroxide (H_2O_2), glutaraldehyde ($CH_2(CH_2CHO)_2$, GTA), phosphate buffered saline (PBS), L-cysteine ($C_3H_7NO_2S$), cysteamine hydrochloride ($C_2H_7NS{\cdot}HCl$), 3-amino-1-propanethiol hydrochloride ($C_3H_9NS{\cdot}HCl$), 6-amino-1-hexanethiol hydrochloride ($C_6H_{15}NS{\cdot}HCl$), 8-amino-1-octanethiol hydrochloride ($C_8H_{19}NS{\cdot}HCl$), 1,3-propanedithiol ($C_3H_8S_2$), 1,6-hexanedithiol ($C_6H_{14}S_2$), 1,9-nonanedithiol ($C_9H_{20}S_2$), and gold(III) chloride hydrate ($HAuCl_4{\cdot}H_2O$) were purchased from Sigma-Aldrich (Australia) and used as received, without further purification. L-Cysteine methyl ester hydrochloride ($C_4H_9NO_2S{\cdot}HCl$) was purchased from TCI Co., Ltd., and used as received, without further purification. AlaAlaCys (AAC) was synthesized by stepwise coupling of Fmoc-Cys (Trt) and Fmoc-Ala amino acids through a standard solid phase synthesis with *N*-fluorenylmethyloxycarbonyl/cysteine(trityl) (N-Fmoc/Cys(Trt)) protecting group strategy (see Supporting Information for further details about the synthesis of the tripeptide AAC). Ethanol (C_2H_5OH, EtOH) and phosphoric acid (H_3PO_4) were supplied by ChemSupply (Australia). Ultrapure water Option Q-Purelabs (Australia) was used in the preparation of aqueous solutions for this study.

2.2. Fabrication of Nanoporous Anodic Alumina (NAA) Platforms. Al substrates were anodized through a two-step electrochemical anodization process reported elsewhere.[28−31] In brief, square-like Al chips 1.5 × 1.5 cm^2 were sonicated in EtOH and ultrapure water for 15 min, respectively, and then dried under air stream. Before anodization, Al chips were electropolished in a mixture of EtOH and $HClO_4$ 4:1 (v:v) at 20 V and 5 °C for 3 min. The first anodization step was performed in an aqueous solution 0.3 M oxalic acid at 40 V and 6 °C for 20 h. The resulting NAA layer was subsequently removed by

DOI: 10.1021/acsami.7b01116
ACS Appl. Mater. Interfaces XXXX, XXX, XXX−XXX

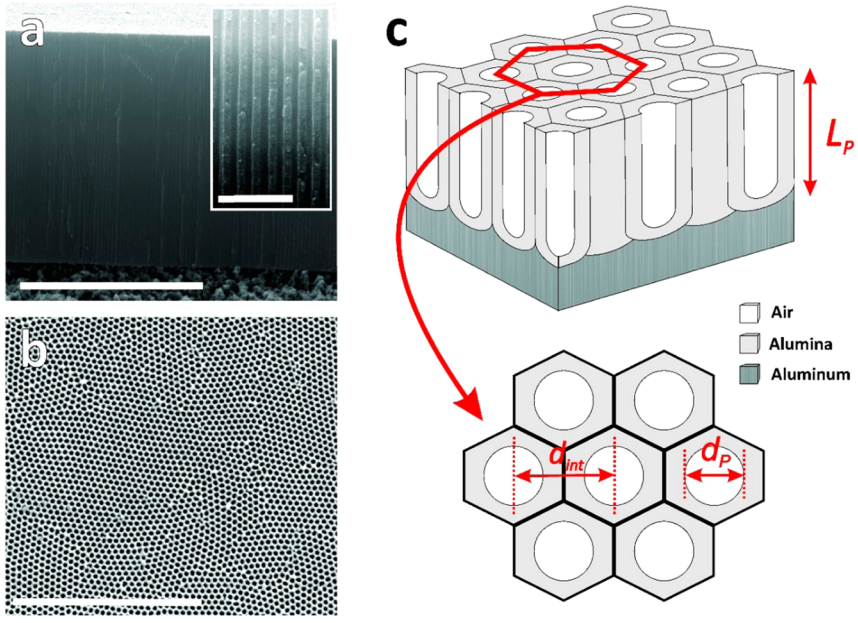

Figure 2. Structural characterization of NAA sensing platforms used in our study. (a) Cross-sectional SEM view of a NAA platform showing straight cylindrical nanopores from top to bottom (scale bar = 5 μm) and inset showing detail of the cylindrical nanopores (scale bar = 500 nm). (b) Top SEM view of a NAA platform featuring characteristic hexagonally arranged cylindrical nanopores across its surface as a result of a two-step anodization process (scale bar = 3 μm). (c) Schematic illustration providing a visual description of the geometric features of NAA platforms with details of the structural parameters (L_p = pore length, d_p = pore diameter, and d_{int} = interpore distance).

wet chemical etching in a mixture of 0.2 M chromic acid (H_2CrO_4) and 0.4 M H_3PO_4 at 70 °C for 3 h. The second anodization step was carried out under the same conditions (0.3 M $H_2C_2O_4$, 40 V and 6 °C) for 2 h. Lastly, the nanoporous structure of these NAA platforms was widened by wet chemical etching in an aqueous solution of H_3PO_4 (5 wt %) at 35 °C for 15 min.

2.3. Surface Chemistry Modification Using Amino-Thiol Functional Molecules: Sensing Approach (i). The functionalization of the inner surface of NAA sensing platforms was carried out via silanization with APTES.[32−35] The as-produced NAA sensing platforms were first hydroxylated by immersion in hydrogen peroxide (30 wt %) at 90 °C for 10 min and then dried under air stream. Next, hydroxylated NAA platforms were functionalized with 3-aminopropyltriethoxysilane by chemical vapor deposition at 110 °C for 3 h and then washed with ethanol and distilled water. To activate the amine terminal group ($-NH_2$) of APTES molecules immobilized onto the inner surface of NAA platforms, these were fully immersed in an aqueous solution of 2.5 vol % glutaraldehyde in PBS for 30 min. GTA-activated NAA sensing platforms were then ready for the immobilization of amino-thiol functional molecules, which was carried out by immersing these platforms into different amino-thiol solutions for 18−20 h. Table 1 summarizes all the thiol-containing functional molecules used in this study. Two parameters of the functional molecules were analyzed using sensing approach (i): namely, the molecular features of amino-thiol molecules and their size. To analyze the former parameter, GTA-activated APTES-functionalized NAA platforms were functionalized with 1 mg mL^{-1} in PBS solution (pH = 7.4) of L-cysteine, cysteamine hydrochloride, L-cysteine methyl ester hydrochloride, and AAC, following the above-mentioned process (*vide supra*). As far as the analysis on the molecular size is concerned, GTA-activated APTES-functionalized NAA platforms were functionalized with 1 mg mL^{-1} in PBS solution of 3-amino-1-propanethiol hydrochloride, 6-amino-1-hexanethiol hydrochloride, and 8-amino-1-octanethiol hydrochloride. Note that amino-thiol-functionalized NAA platforms were washed with ultrapure water and dried under air stream after functionalization. Finally, the amino-thiol-functionalized NAA sensing platforms were coated with an ultrathin layer of gold (i.e., 4−5 nm) using a sputter coater equipped with a film thickness monitor (sputter coater 108auto, Cressington, USA) to enhance light interference.[16,21]

2.4. Surface Chemistry Modification Using Dithiol Molecules: Sensing Approach (ii). The top surface of gold-coated NAA sensing platforms was selectively functionalized with a set of dithiol molecules (Table 1) by direct immersion in a solution of functionalizing molecules over 18−20 h to generate self-assembled monolayers of dithiol molecules onto gold sputtered onto the top surface of NAA platforms. The dithiol solutions used were 1 mg mL^{-1} of 1,3-propanedithiol, 1,6-hexanedithiol, and 1,9-nonanedithiol in EtOH. The dithiol-functionalized NAA platforms were then washed with EtOH and ultrapure water after functionalization to remove physisorbed molecules, dried under air stream, and stored under dry conditions until further use.

2.5. Surface Chemistry Modification Using Both Amino-Thiol and Dithiol Molecules: Sensing Approach (iii). After establishing the most sensitive thiol-containing functional molecules in approaches (i) and (ii) (i.e., amino-thiols and dithiols, respectively), a set of NAA platforms were selectively functionalized with both thiol-terminated molecules, sequentially. In this process, NAA platforms were first hydroxylated, silanized, and activated using the above-mentioned silanization protocol. The GTA-activated APTES-functionalized NAA platforms were then ready for the selective immobilization of amino-thiol molecules onto the inner surface of their nanopores, which was carried out under batch condition (i.e., immersion of NAA platforms in amino-thiol solution for 18−20 h). The amino-thiol-functionalized NAA platforms were then coated with a thin layer of gold, and their top surface was selectively functionalized with dithiol molecules under batch conditions for 18−20 h following the protocol used in approach (ii).

2.6. RIfS System and Detection of Gold Ions (Au^{3+}). Details of our RIfS setup have been reported elsewhere.[20,22] In brief, white light from a tungsten source was directed onto the surface of thiol-functionalized NAA platforms with an illumination spot of 2 mm by a bifurcated optical probe. The collection fiber of the optical probe collected and transferred the reflected light from the illumination spot to a miniature spectrophotometer (USB 4000 + VIS-NIR-ES, Ocean Optics, USA). The optical spectra were obtained in the range 400−1000 nm and saved at intervals of 30 s with an integration time of 20 s, with 20 average measurements. The acquired RIfS spectra were

DOI: 10.1021/acsami.7b01116
ACS Appl. Mater. Interfaces XXXX, XXX, XXX−XXX

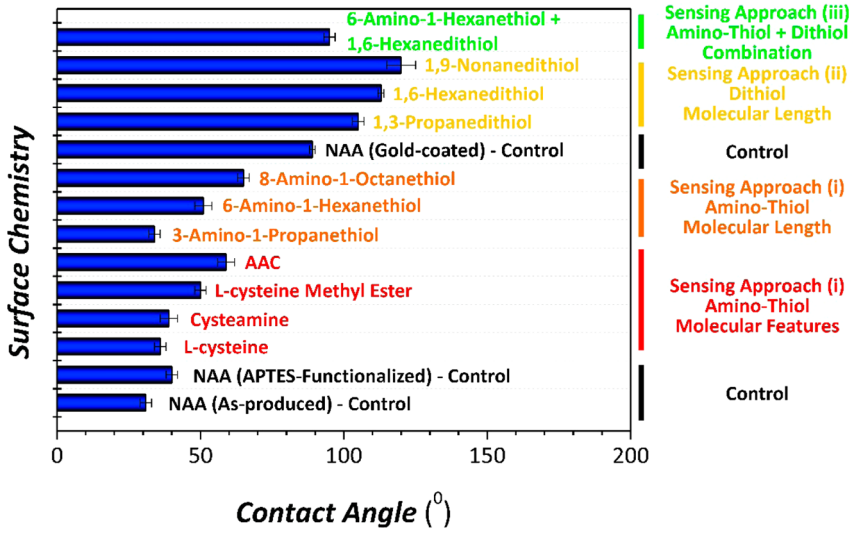

Figure 3. Contact angle characterization for the different surface chemistries assessed in our study.

processed by applying fast Fourier transform using Igor Pro library (Wavemetrics, USA) to estimate the effective optical thickness (OT_{eff}) of the NAA sensing platforms (eq 1):

$$OT_{eff} = 2n_{eff}L_p \cos\theta \quad (1)$$

where OT_{eff} is the effective optical thickness of the film, n_{eff} is the effective refractive index of the NAA platform, L_p is its physical thickness, and θ is the angle of incidence of light (i.e., $\theta = 0°$ in this case).

The sensitivity of thiol-functionalized NAA platforms toward gold ions was assessed by RIfS through changes in OT_{eff} as a function of the concentration of gold ions. This binding process was monitored in real time using a custom-designed flow cell. A stock solution of Au^{3+} ions (1 mM) was prepared by dissolving $HAuCl_4 \cdot H_2O$ in ultrapure water, and analytical solutions of Au^{3+} with concentrations ranging from 20 to 80 μM with an interval of 20 μM were obtained by dilution of the Au^{3+} stock solution. Thiol-functionalized NAA sensing platforms were packed in a custom-made flow cell based on transparent acrylic plastic and analytical solutions were flowed at a rate of 100 μL min^{-1}. This flow rate was maintained throughout the sensing experiments by a peristaltic pump (LongerPump BT100-2J) with an equivalent pumping angular rate of 1.4 rpm. The sensing experiments started with the establishment of stable baseline by flowing ultrapure water. Once a stable baseline was obtained, analytical solutions of Au^{3+} of different concentrations (20, 40, 60, and 80 μM) were introduced into the flow cell. The interaction between Au^{3+} ions present in the analytical solutions and thiol functional groups on the surface of functionalized NAA platforms induced sharp changes (i.e., increment = red-shift) in the OT_{eff} of NAA platforms. After OT_{eff} achieved a stable value, ultrapure water was flowed for 15 min to obtain the total change of OT_{eff} (ΔOT_{eff}) associated with the corresponding concentration of Au^{3+} ions. Note that fresh thiol-functionalized NAA platforms were used to establish the total effective optical thickness change for each analytical concentration of Au^{3+}.

2.7. Structural Characterization of NAA Sensing Platforms. Scanning electron microscopy (SEM) images of NAA sensing platforms were acquired using a field-emission gun scanning electron microscopy (FEG-SEM FEI Quanta 450). These images were used to establish the geometric features of NAA platforms by image analysis using ImageJ (public domain program developed at the RSB of the NIH).[36]

2.8. Contact Angle Measurement in NAA Sensing Platforms. The contact angle for each NAA sensing platforms was measured by a tensiometer (Attension Theta optical tensiometer). The sensile drop technique was used in these experiments, where a water droplet was formed on the end of a syringe, which was descended until the water droplet touched the surface of the sample stage, followed by the withdraw of the needle away from the stage. Image analysis was used to establish the contact angle on the surface of NAA platforms containing functional groups.

3. RESULTS AND DISCUSSION

3.1. Structural Characterization of NAA Sensing Platforms. SEM images of the NAA platforms reveal the characteristic geometric features of NAA produced by a two-step anodization approach (Figure 2). Cross-sectional SEM images of these platforms show vertically aligned straight cylindrical nanopores from top to bottom (Figure 2a). Top SEM images reveal that these nanoporous photonic films feature hexagonally arranged nanopores homogeneously distributed across their surface (Figure 2b) with an average pore diameter (d_p) of 66 ± 6 nm, pore length (L_p) of 6.0 ± 0.1 μm, and interpore distance (d_{int}) of 105 ± 4 nm (Figure 2c).

3.2. Contact Angle Measurements of Functionalized NAA Sensing Platforms. The successful functionalization of NAA platforms with thiol-containing functional molecules using approaches (i) and (ii) was validated and analyzed by contact angle measurements (Figure 3). Note that the purpose of contact angle measurements was to establish the effect of the molecular interaction and conformation among the functionalizing molecules on the hydrophobic character of functionalized NAA platforms. As such, these NAA platforms for sensing approach (i) were not coated with a thin layer of gold to mimic the surface chemistry inside the nanopores. Two samples were used as control references for NAA platforms functionalized following approach (i) (i.e., selective functionalization of the inner surface of the nanopores with amino-thiol functional molecules), being the as-produced and APTES-functionalized NAA platforms. The contact angle of these NAA platforms was found to be 31 ± 2° and 40 ± 2°, respectively. Whereas as-produced NAA platforms have a hydrophilic character, the functionalization of their inner surface with APTES molecules induces a relatively weak hydrophobic character due to the presence of amine terminal groups ($-NH_2$) (Figure 3). As for the effect of the molecular features of cysteine-like molecules, Figure 3 shows that the hydrophobic character of the NAA increases in the following order: L-cysteine (36 ± 2°) < cysteamine (39 ± 3°) < L-cysteine methyl

DOI: 10.1021/acsami.7b01116
ACS Appl. Mater. Interfaces XXXX, XXX, XXX−XXX

ester (50 ± 2°) < AAC (59 ± 3°). These results show that the presence of additional functional groups (e.g., carboxyl, ester, methyl, etc.) has a significant impact on the hydrophobic character of these photonic films (Table 1). For instance, AAC is a tripeptide and thus possesses two amide functional groups. As a result, AAC-functionalized NAA platforms have the strongest hydrophobic character among the cysteine-like functional molecules analyzed in our study. This property in turn determines the surface interaction between analyte molecules (i.e., Au^{3+}) in an aqueous matrix and the surface of the sensing platforms. Another important factor which plays a role in the overall hydrophobic character of functionalized NAA platforms is the length of the functional molecules. To discern the effect of this parameter, we analyzed the contact angle in a set of NAA platforms functionalized with amino-thiol molecules (Figure 3 and Table 1). Our results reveal that the hydrophobic character of NAA platforms increases with the length of the amino-thiol functional molecules in the following order: 3-amino-1-propanethiol (34 ± 2°) < 6-amino-1-hexanethiol (51 ± 3°) < 8-amino-1-octanethiol (65 ± 2°) (Figure 3 and Table 1). As such, the longer the amino-thiol backbone, the more hydrophobic the character of the functionalized surface. It is worthwhile noting that thiol groups (−SH) are hydrophobic. Therefore, the conformation of the functional layer immobilized onto the surface of NAA has a direct effect upon the overall hydrophobic character of these films. This result suggests that functional layers of 8-amino-1-octanethiol molecules immobilized onto the inner surface of GTA-activated APTES-functionalized NAA platforms have a more compact assembly as compared to other functional amino-thiol molecules of shorter backbone structure. As such, more thiol functional terminal groups would be exposed across the surface of NAA, increasing the hydrophobic character of NAA platforms functionalized with 8-amino-1-octanethiol.

Finally, we assessed the contact angle of NAA films functionalized with dithiol molecules following approach (ii). In this case, a gold-coated NAA platform was used as a control, the contact angle of which was found to be significantly more hydrophobic (i.e., 89 ± 1°) than that of noncoated or amino-thiol-functionalized NAA platforms (Figure 3). The hydrophobic character of these NAA platforms was further increased after selective chemical functionalization with dithiol groups following sensing approach (ii) (Figure 1a). We also analyzed the effect of the length of dithiol molecules on the hydrophobic character of NAA platforms. Our results demonstrate that as per the amino-thiol molecules, longer molecules give a more hydrophobic character to the NAA platform in the following order: 1,3-propanedithiol (105 ± 2°) < 1,6-hexanedithiol (112 ± 1°) < 1,9-nonanedithiol (119 ± 5°). Therefore, this result verifies that longer molecules can provide more compact self-assembled monolayers of dithiol functional groups onto the surface of gold-coated NAA platforms.

3.3. Evaluation of Sensitivity in NAA Sensing Platforms Functionalized with Amino-Thiol Functional Molecules. A range of amino-thiol molecules containing a common cysteine-like backbone structure was used to modify the surface chemistry of NAA platforms and discern the effect of molecular functionalities and backbone length on the sensing performance of NAA interferometric sensors. Prior to immobilization, silanization and activation of amine terminal groups were performed. In this process, NAA platforms were pretreated with hydrogen peroxide for hydroxylation of the inner surface of nanopores (i.e., generation of hydroxyl groups). Silanization of these NAA platforms was carried out by chemical vapor deposition of APTES molecules to endow as-produced NAA platforms with amine functionality through the silane layer, inside the nanopores.[37] The amine functional groups of APTES molecules were then activated by GTA molecules, which provides aldehyde functionality, through the immersion of NAA platforms in GTA solution. The immobilization of amino-thiol molecules on the GTA-activated NAA platforms occurred through the amine binding formed between the aldehyde functionality of GTA molecules and the amine group of amino-thiol molecules.[37] A schematic illustration of the immobilization and binding of these molecules onto the inner surface of GTA-activated APTES-functionalized NAA platforms is shown in Figure 1c. Both the inner and top surfaces of the NAA were functionalized with APTES, GTA, and amino-thiol molecules. Note that these amino-thiol-functionalized NAA platforms were coated with a thin layer of gold before they were used as sensing platforms. This layer of gold covered the functional molecules attached onto the top surface of NAA platforms, preventing top surface functional groups from interacting with Au^{3+} ions. Thus, there was no occurrence of binding events on the top surface of NAA platforms, and only amino-thiol molecules functionalized on the inner surface of nanopores were exposed to Au^{3+} ions for binding.

3.3.1. Effect of Molecular Features in Amino-Thiol Functional Molecules. The cysteine-like molecules immobilized onto the inner surface of NAA platforms have similar backbone structure, where they have both amine and thiol groups, but they differ in their functional groups along the molecule (e.g., carboxyl, ester, etc.), as shown in Table 1. These amino-thiol functionalized NAA sensing platforms were combined with RIfS and their sensitivity assessed by measuring changes in the effective optical thickness of the film (ΔOT_{eff}) in response to the binding of Au^{3+} ions present in analytical solutions of different concentration (20, 40, 60, and 80 μM) using sensing approach (i) (Figure 1a). Figure 4a displays representative graphs showing ΔOT_{eff} as a function of time for NAA platforms functionalized with L-cysteine, cysteamine, L-cysteine methyl ester, and AAC. Note that a stable baseline was first obtained in ultrapure water before injection of the analyte solution containing Au^{3+} ions. An increase in OT_{eff} was observed as the Au^{3+} solution was flowed through the system, which indicates the binding between Au^{3+} ions and thiol functional groups immobilized onto the inner surface of these NAA platforms. This observation is true for all cases (i.e., L-cysteine, cysteamine, and AAC) except for L-cysteine methyl ester, where there was a decrease in OT_{eff} at the initial stage of the flowing of Au^{3+} solution. The decrease in OT_{eff} observed might be due to conformational changes upon the interaction between Au^{3+} and L-cysteine methyl ester. Ultrapure water was flowed again through the system for 15 min once the binding between gold ions and thiol groups reached the equilibrium, which was characterized by a plateau in the spectra. In this process, ΔOT_{eff} was found to decrease slightly due to the removal of physisorbed gold ions, which is in good agreement with previous studies using a similar sensing approach.[22] The correlation between ΔOT_{eff} and the concentration of Au^{3+} for cysteine-like molecules with different molecular features is shown in Figure 4b. This analysis reveals a linear dependence of ΔOT_{eff} with $[Au^{3+}]$ for all the cysteine-like molecules within the range of concentrations studied. As the concentration of gold ions in the analytical solution increases, more Au^{3+} ions

DOI: 10.1021/acsami.7b01116
ACS Appl. Mater. Interfaces XXXX, XXX, XXX−XXX

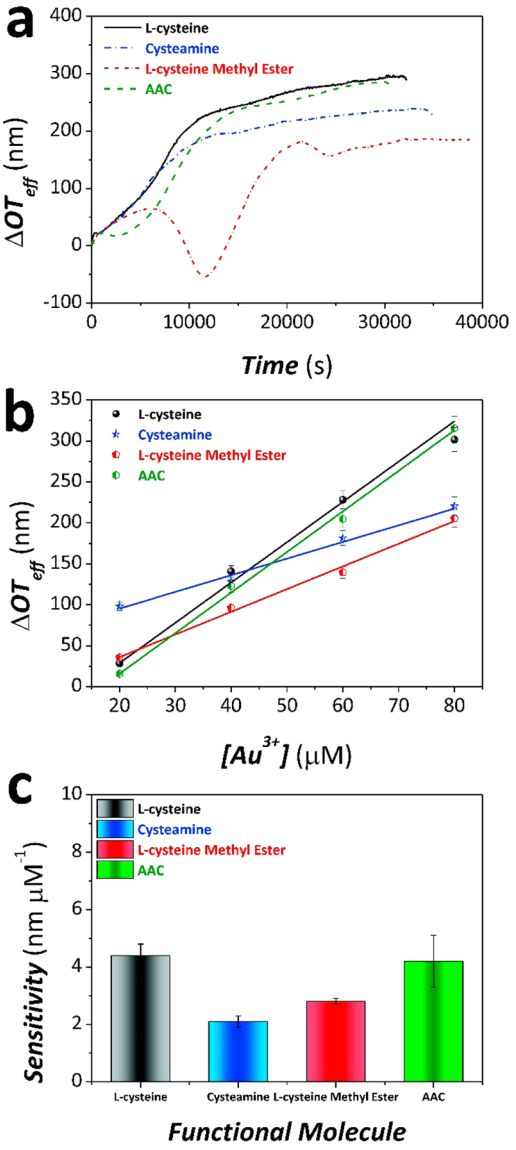

Figure 4. Assessment of optical sensitivity for amino-thiol functional molecules with different molecular features in NAA sensing platforms through the detection of different concentrations of gold ions using sensing approach (i). (a) Representative graph showing the effective optical thickness change in NAA sensing platforms functionalized with L-cysteine, cysteamine, L-cysteine methyl ester, and AAC for a concentration 80 μM of Au^{3+} measured in real time by RIfS. (b) Linear fitting lines for NAA sensing platforms modified with L-cysteine, cysteamine, L-cysteine methyl ester, and AAC used to establish the linear correlation between ΔOT_{eff} and $[Au^{3+}]$ for the range of concentrations 20, 40, 60, and 80 μM. (c) Bar chart summarizing the sensitivities (i.e., slope of linear fittings shown in (b)) for NAA sensing platforms modified with L-cysteine, cysteamine, L-cysteine methyl ester, and AAC.

are available to be bound by thiol functional groups present in the inner surface of NAA platforms, which in turn is translated into greater changes in the effective optical thickness. The slope of these linear fittings corresponds to the sensitivity of the system, expressed in terms of effective optical thickness change per concentration unit (i.e., nm μM^{-1}) (Figure 4c). Our results indicate that L-cysteine and AAC provide approximately the same level of sensitivity to Au^{3+} ions (4.4 $\pm$ 0.4 and 4.2 $\pm$ 0.6 nm μM^{-1}, respectively), whereas NAA platforms functionalized with L-cysteine methyl ester and cysteamine show the least sensitivity (i.e., 2.8 $\pm$ 0.1 and 2.1 $\pm$ 0.2 nm μM^{-1}, respectively). Unlike the other amino-thiol molecules, the only site for cysteamine molecules to interact with Au^{3+} ions is via the thiol terminal group. Thus, the amount of gold ions immobilized onto the inner surface of NAA platforms is approximately equivalent to the number of cysteamine molecules available inside the surface of NAA nanopores. As a result, the low sensitivity achieved by cysteamine-functionalized NAA platforms when detecting gold ions (2.1 $\pm$ 0.2 nm μM^{-1}) could be associated with the lack of other functionalities along its backbone structure, which might provide further sites for binding interactions. Although L-cysteine methyl ester possesses a terminal-ester functional group, the presence of this additional functional group compared to L-cysteine only slightly improves the sensitivity of the NAA platforms toward Au^{3+} ions (2.8 $\pm$ 0.1 nm μM^{-1}), as revealed by the results shown in Figure 4c. In contrast to cysteamine and L-cysteine methyl ester, the carboxylic acid groups of L-cysteine and AAC might be able to interact with gold ions through van der Waals forces, increasing the occurrence of gold ion capturing events inside the nanopores and thus enhancing the overall sensitivity of the system as a result (i.e., 4.4 $\pm$ 0.4 and 4.2 $\pm$ 0.6 nm μM^{-1}, respectively). Carboxylic acid is known as one of the common building blocks for the formation of molecular self-assembled layers on metal surfaces through chemisorption.[38] Therefore, we suggest that L-cysteine and AAC molecules immobilized onto the inner surface of NAA nanopores could also bind to areas that are free of APTES linkage molecules through the direct chemisorption of carboxylic acid on APTES-free aluminum oxide.[39] This would result in an increment in the number of thiol-terminated molecules present on the inner surface of NAA nanopores, which in turn would be translated into a significant enhancement of the sensitivity of the NAA platforms toward Au^{3+} ions. As mentioned before, the size and the refractive index of the functional molecules immobilized onto the inner surface of NAA platforms could also have an impact on the overall sensitivity of the system.[25] It can be observed that whereas cysteamine has the smallest chemical structure among the functional molecules analyzed in this section of our study, the functional molecule AAC has the biggest molecular size, which could contribute to a more sensitive system due to the bigger magnitude of the ΔOT_{eff} in NAA platforms when interacting with Au^{3+} ions.

3.3.2. Effect of Molecular Length in Amino-Thiol Functional Molecules. NAA sensing platforms were functionalized with amino-thiol molecules featuring different backbone lengths by APTES silanization and subsequent immobilization by GTA activation and functionalization of amino-thiol molecules. These NAA platforms were then gold coated before being used as sensing platforms. The amino-thiol molecules used in our study to assess the effect of the molecular length by sensing approach (i) were 3-amino-1-propanethiol, 6-amino-1-hexanethiol, and 8-amino-1-octanethiol. As depicted in Table 1, these molecules possess a terminal amine group ($-NH_2$), which is responsible for attachment to the GTA-activated APTES molecules immobilized onto the inner surface of NAA nanopores. Additionally, a terminal thiol group ($-SH$) is responsible for Au^{3+} ions capture, and the sole variation between these amino-thiol molecules is the length of the carbon chain between the terminal functional groups. Assessment of the sensitivity of these amino-thiol-functionalized NAA platforms was carried out using the protocol outlined

DOI: 10.1021/acsami.7b01116
ACS Appl. Mater. Interfaces XXXX, XXX, XXX−XXX

previously based on sensing approach (i) (Figure 1a). Figure 5a shows an example of real-time sensing in these NAA-

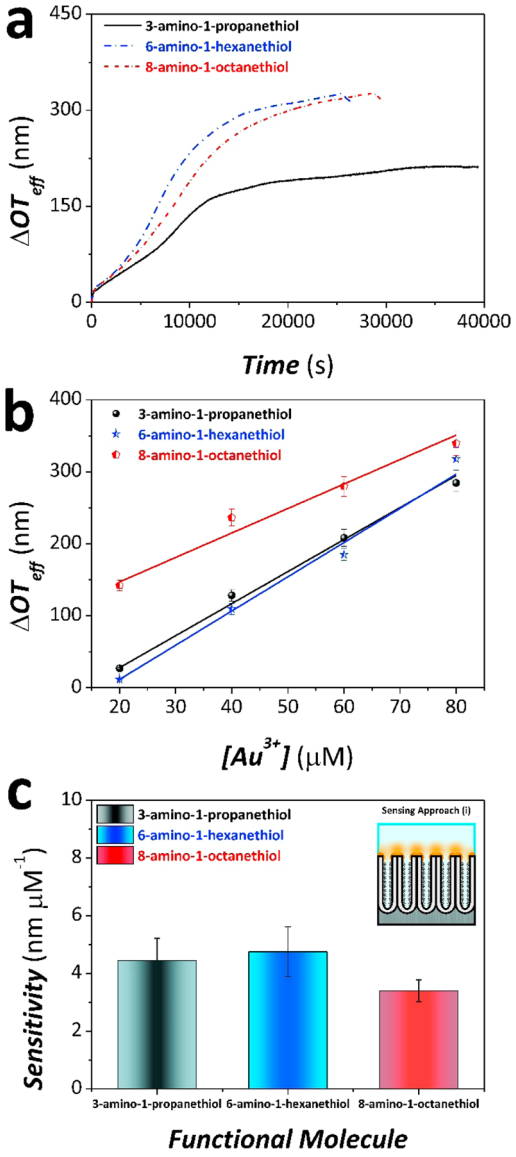

Figure 5. Assessment of optical sensitivity for amino-thiol functional molecules with different molecular lengths in NAA sensing platforms through the detection of different concentrations of gold ions using sensing approach (i). (a) Representative graph showing the effective optical thickness change in NAA sensing platforms functionalized with 3-amino-1-propanethiol, 6-amino-1-hexanethiol, and 8-amino-1-octanethiol for a concentration 80 μM of Au^{3+} measured in real time by RIfS. (b) Linear fitting lines for NAA sensing platforms modified with 3-amino-1-propanethiol, 6-amino-1-hexanethiol, and 8-amino-1-octanethiol used to establish the linear correlation between ΔOT_{eff} and $[Au^{3+}]$ for the range of concentrations 20, 40, 60, and 80 μM. (c) Bar chart summarizing the sensitivities (i.e., slope of linear fittings shown in (b)) for NAA sensing platforms modified with 3-amino-1-propanethiol, 6-amino-1-hexanethiol, and 8-amino-1-octanethiol.

functionalized platforms, while Figure 5b depicts the correlation between Au^{3+} ions concentration and ΔOT_{eff}, establishing the linear dependency of ΔOT_{eff} for amino-thiol-functionalized NAA platforms with $[Au^{3+}]$. It is apparent that the higher the concentration of gold ions in the analyte solution, the more Au^{3+} ions available to interact with amino-thiol molecules immobilized onto the inner surface of NAA nanopores. As such, ΔOT_{eff} increases with the concentration of gold ions, linearly, within the range of analyte concentrations used in our study. The sensitivity provided by these amino-thiol molecules of different molecule length was estimated by the slope of the fitting lines for the respective amino-thiol molecules shown in Figure 5b. An overview of the sensitivity of these amino-thiol molecules is presented in the bar chart of Figure 5c. Our analysis reveals that NAA platforms functionalized with 6-amino-1-hexanethiol have the greatest sensitivity (4.8 ± 0.9 nm μM^{-1}) followed by 3-amino-1-propanethiol (4.4 ± 0.8 nm μM^{-1}). Interestingly, 8-amino-1-octanethiol-functionalized NAA platforms showed the least sensitivity toward Au^{3+} ions (3.4 ± 0.4 nm μM^{-1}). Previous studies indicated that functional molecules of bigger molecular size immobilized onto the inner surface of nanoporous materials can provide more significant changes in the effective optical thickness of the sensing platforms, resulting in a higher sensitivity toward targeted analytes.[26,27] Nevertheless, we found this to be partly true for NAA platforms functionalized with 3-amino-1-propanethiol and 6-amino-1-hexanethiol, where the latter (i.e., 6C) is slightly more sensitive toward Au^{3+} ions as compared to the former (i.e., 3C). However, 8-amino-1-octanethiol was the least sensitive molecule, despite being the longest (i.e., 8C) of those investigated. This might be due to the molecular orientation and conformation of 8-amino-1-octanethiol immobilized onto the inner surface of NAA nanopores. The longer carbon chain length of 8-amino-1-octanethiol might lead to molecules becoming folded or crumpled up inside the nanopores, shielding the thiol functional groups from interacting with Au^{3+} ions. In contrast, the shorter lengths of 3-amino-1-propanethiol and 6-amino-1-hexanethiol molecules could facilitate the orientation and alignment in such a way that the amount of sensing molecules and available thiol functional groups inside the nanopores is higher than that of 8-amino-1-octanethiol molecules. Based on these observations, we postulate that there is an optimal size in terms of overall sensitivity of the system for the functionalizing molecules to be immobilized onto the inner surface of NAA nanopores.

3.4. Evaluation of Sensitivity of NAA Sensing Platforms Functionalized with Dithiols of Different Molecular Sizes toward Au^{3+} Ions. Sensing approach (ii) corresponds to a localized surface plasmon resonance (LSPR) sensing configuration (Figure 1b). It is known that a LSPR approach in NAA sensing platforms can provide high sensitivity and low limit of detection performances due to the disturbance and interaction between the electromagnetic field generated around nanometric metallic structures and analyte molecules.[40,41] In our study, NAA sensing platforms were coated with a thin layer of gold before functionalization with dithiol molecules of different molecular length (i.e., carbon chain). The dithiol molecules used in this study feature different backbone lengths, 1,3-propanedithiol (3C), 1,6-hexanedithiol (6C), and 1,9-nonanedithiol (9C). The chemical structures of the dithiol molecules possess a terminal thiol group at each end of the molecule as shown in Table 1. Unlike the previous sensing approach where the amino-thiol molecules were selectively immobilized inside the NAA nanopores, these dithiol molecules were selectively attached on the top surface of gold-coated NAA nanopore through the well-known affinity interaction between gold on the surface of NAA and one of the thiol groups of the dithiol molecules. The other thiol group remains free to detect Au^{3+} ions during the flow of analyte solutions.

DOI: 10.1021/acsami.7b01116
ACS Appl. Mater. Interfaces XXXX, XXX, XXX−XXX

The attachment of dithiol molecules on the gold-coated surface of NAA is illustrated in Figure 1b. An example of real-time sensing and the resulting linear correlation between the concentration of Au^{3+} ions and ΔOT_{eff} for each dithiol molecule is presented in Figure 6a,b. These results indicate that ΔOT_{eff} increases linearly with the concentration of gold ions present in the analyte solutions. As the concentration of Au^{3+} increases, there are more gold ions available to be captured by dithiol molecules attached on the surface of NAA. As a result, the occurrence of gold−thiol binding events on the gold-coated surface of NAA increases, producing a greater ΔOT_{eff} of the film. Figure 6b shows the linear fittings corresponding to the different NAA sensing platforms functionalized with the dithiol molecules used in our study. These fittings were used to assess the sensitivity of these dithiol molecules toward gold ions using sensing approach (ii). As indicated by the bar chart in Figure 6c, NAA platforms functionalized with 1,6-hexanedithiol are the most sensitive platforms toward Au^{3+} ions, with a sensitivity of 0.9 ± 0.1 nm μM^{-1}, whereas 1,3-propanedithiol and 1,9-nonanedithiol have significantly poorer sensitivity of 0.3 ± 0.1 and 0.2 ± 0.1 nm μM^{-1}, respectively. In the LSPR approach used in our study, the gold−thiol binding events taking place on the gold-coated surface of NAA platforms induce a change in the local refractive index environment, which is measured through changes in effective optical thickness of the film by RIfS. It is worth noting that the electromagnetic fields near the metal surface are greatly enhanced; however, the electromagnetic strength decreases rapidly with the distance from the metallic structure (Figure 1b). Therefore, it is expected that the sensitivity of NAA sensing platforms using sensing approach (ii) will increase if they are functionalized with dithiol molecules of smaller molecular size. Duyne and co-workers demonstrated the reduction of LSPR sensitivity with distance from the surface of metallic structures using self-assembled monolayers of increasing length.[42−44] Dithiols of shorter chain length present the thiol terminal group inside the strongest part of the electromagnetic field generated on the gold-coated surface of NAA (Figure 1b). Therefore, gold−thiol binding events occurring within that part of the localized electromagnetic field can significantly change the overall effective optical thickness of the platform. NAA platforms functionalized with 1,9-nonanedithiol exhibit low sensitivity, and this might be due to the fact that the thiol group responsible for the interaction with Au^{3+} ions is located far from the active zone of the local electromagnetic field, where its strength is poor. Thus, changes in the local refractive index environment due to gold−thiol interaction are not optimal to be translated into changes in the effective optical thickness of the film, as indicated by the low sensitivity achieved in these NAA platforms. In contrast, NAA platforms functionalized with 1,6-hexanedithiol exhibited the highest sensitivity, indicating that the binding between thiol and Au^{3+} ions occurs at a distance where the electromagnetic field presents the highest strength. NAA platforms functionalized with 1,3-propanedithiol had a low sensitivity probably due to the decay in the strength of the electromagnetic field.

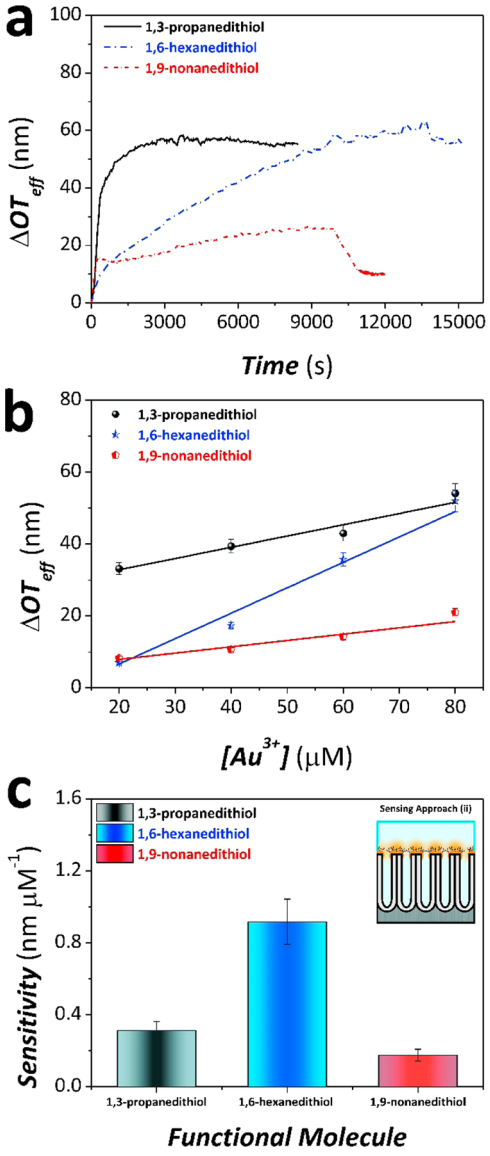

Figure 6. Assessment of optical sensitivity for dithiol functional molecules with different molecular lengths in NAA sensing platforms through the detection of different concentrations of gold ions using sensing approach (ii). (a) Representative graph showing the effective optical thickness change in NAA sensing platforms functionalized with 1,3-propanedithiol, 1,6-hexanedithiol, and 1,9-nonanedithiol for a concentration 80 μM of Au^{3+} measured in real time by RIfS. (b) Linear fitting lines for NAA sensing platforms modified with 1,3-propanedithiol, 1,6-hexanedithiol, and 1,9-nonanedithiol used to establish the linear correlation between ΔOT_{eff} and $[Au^{3+}]$ for the range of concentrations 20, 40, 60, and 80 μM. (c) Bar chart summarizing the sensitivities (i.e., slope of linear fittings shown in (b)) for NAA sensing platforms modified with 1,3-propanedithiol, 1,6-hexanedithiol, and 1,9-nonanedithiol.

It is noteworthy that sensitivities of NAA sensing platforms modified with dithiol molecules using sensing approach (ii) were significantly lower than that of amino-thiol molecules using sensing approach (i). Our results also indicate that the required time for the binding of Au^{3+} ions to dithiol molecules immobilized on the gold-coated surface of NAA platforms to reach equilibrium was shorter than that of amino-thiol molecules selectively immobilized inside the nanopores. This might be associated with the presence of more thiol functional groups on the surface of NAA platforms. The top surface area used in sensing approach (ii) with dithiol molecules is much smaller than that of the inner surface of NAA nanopores used in sensing approach (i) for the immobilization of amino-thiol molecules. As a result, less gold−thiol binding events occur on the gold-coated dithiol-functionalized surface of NAA plat-

DOI: 10.1021/acsami.7b01116
ACS Appl. Mater. Interfaces XXXX, XXX, XXX−XXX

forms, and thus changes in the effective optical thickness of these NAA platforms are smaller, resulting in lower sensitivities.

3.5. Evaluation of Sensitivity of NAA Sensing Platforms with Dual Functionalization. We performed a pioneering set of experiments in order to discern whether the implementation of sensing approaches (i) and (ii) into the same NAA platform results in an additive enhancement of the overall sensitivity of the system. To this end, NAA sensing platforms were functionalized on both the inner surface of NAA nanopores as well as the gold-coated surface of NAA platforms (sensing approach (iii) as illustrated in Figure 1a) using the most sensitive molecules identified from sensing approaches (i) and (ii). 6-Amino-1-hexanethiol (inner surface) and 1,6-hexanedithiol (top surface), with individual sensitivities of 4.8 ± 0.9 and 0.9 ± 0.1 nm μM^{-1}, respectively, were used as sensing molecules for sensing approach (iii). Following hydroxylation and silanization, NAA sensing platforms were functionalized with 6-amino-1-hexanethiol. The amino-thiol modified NAA platforms were then coated with gold before selective functionalization of their top surface with 1,6-hexanedithiol molecules. The dual-functionalized NAA platforms were then used in the detection of gold ions by RIfS. The obtained results presented in Figure 7a,b show that ΔOT_{eff} increases with increasing Au^{3+} in the analyte solution, following a linear relationship between these two parameters. Note that the binding of Au^{3+} to the dual-functionalized NAA platforms took a longer time to reach the equilibrium, which might be due to the presence of functionalizing molecules on the top surface of NAA. The layer of dithiol molecules attached on the top surface of NAA and their interaction with Au^{3+} might act as a hindrance barrier to the flow of Au^{3+} into the nanopores, delaying the occurrence of Au^{3+}–amino-thiol interaction inside the nanopores, thus taking longer time to reach the equilibrium. The sensitivity of NAA platforms using sensing approach (iii) was found to be 5.6 ± 1.0 nm μM^{-1}. Significantly, the combined functionalization of both the inner and top surfaces of NAA platforms provides an almost additive enhancement of the sensitivity compared to that of NAA platforms functionalized with either 6-amino-1-hexanethiol or 1,6-hexanedithiol alone, using sensing approaches (i) and (ii) individually. The sensitivities of these three NAA platforms are compared in Figure 7c. These results indicate that the sensitivity enhancement is approximately additive due to the combined effect of amino-thiol and dithiol molecules selectively immobilized onto NAA platforms. Functionalization of both the inner and top surfaces of NAA nanopores results in more thiol functional groups on the surface of NAA platforms, which are then exposed to gold ions present in the analyte solution. As a result, greater changes in the effective optical thickness of these NAA platforms occur, increasing the overall sensitivity of the system. These results demonstrate that the sensitivity of NAA sensing platforms can be improved by a rational engineering of the surface chemistry. In our case, we found that this rational engineering can make it possible to achieve a 6-fold greater sensitivity than that obtained in previous studies.[21]

4. CONCLUSIONS

We have demonstrated for the first time a rationale toward enhancing sensitivity in thiol-modified NAA sensing platforms by surface chemistry engineering. The surface chemistries of NAA sensing platforms were selectively modified using thiol-containing molecules (i.e., amino-thiol and dithiol molecules) with a range of molecular features and backbone sizes and using

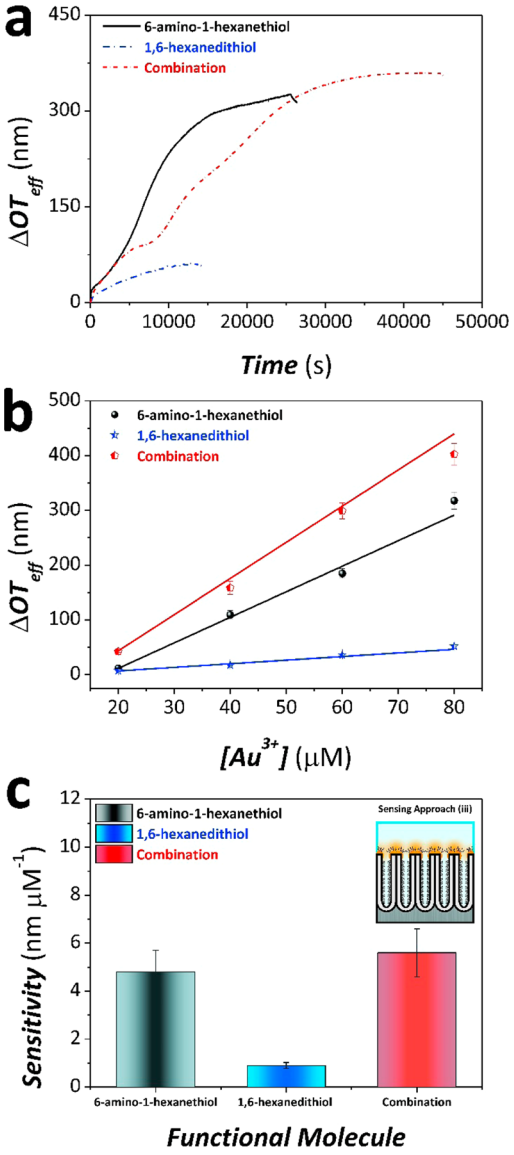

Figure 7. Assessment of optical sensitivity for combined functional molecules in NAA sensing platforms through the detection of different concentrations of gold ions using sensing approach (iii). (a) Representative graph showing the effective optical thickness change in NAA sensing platforms functionalized with 6-amino-1-hexanethiol, 1,6-hexanedithiol, and the combination of both for a concentration 80 μM of Au^{3+} measured in real time by RIfS. (b) Linear fitting lines for NAA sensing platforms modified with 6-amino-1-hexanethiol, 1,6-hexanedithiol, and the combination of both used to establish the linear correlation between ΔOT_{eff} and $[Au^{3+}]$ for the range of concentrations 20, 40, 60, and 80 μM. (c) Bar chart summarizing the sensitivities (i.e., slope of linear fittings shown in (b)) for NAA sensing platforms modified with 6-amino-1-hexanethiol, 1,6-hexanedithiol, and the combination of both.

two different sensing approaches. A series of experiments based on the detection of gold ions were carried out to assess the effect of these functional molecules and the sensing approach on the sensitivity of the system. Changes in the effective optical thickness of these NAA platforms were used as the sensing parameter for the establishment of the overall sensitivity of the system. Our experiments revealed that 6-amino-1-hexanethiol molecules provide the best sensing performance of the amino-thiol modified NAA platforms using sensing approach (i), with

DOI: 10.1021/acsami.7b01116
ACS Appl. Mater. Interfaces XXXX, XXX, XXX−XXX

a sensitivity of 4.8 ± 0.9 nm μM^{-1}. NAA sensing platforms modified with 1,6-hexanedithiol were the most sensitive platform (0.9 ± 0.1 nm μM^{-1}) for dithiol-functionalized NAA platforms using approach (ii). To further enhance the overall sensitivity of the system, NAA sensing platforms were modified using a dual functionalization approach with 6-amino-1-hexanethiol and 1,6-hexanedithiol, as these two molecules offered the best individual sensitivities as compared to other amino-thiol and dithiol molecules. Our results indicated that the sensing performance of the resulting NAA platforms has an additive enhancement of sensitivity (5.6 ± 1.0 nm μM^{-1}) as a result of the combined Au^{3+} ion binding capacity of 6-amino-1-hexanethiol (inner surface) and 1,6-hexanedithiol (top surface).

We have established that the performance of a sensor is dependent on the molecular makeup and backbone length of the functional molecule employed as well as the sensing approach utilized. The sensitivity of a sensing system can be enhanced through a rational engineering of the surface chemistry on the sensing platform, where these interferometric sensing platforms can be functionalized with analyte-specific molecules that respond to the same targeted analytes but may differ in their backbone structures or molecular sizes. Different functional groups or molecular sizes can endow a sensing platform with more sensitivity. In conclusion, our study provides a better understanding and deeper insight into potential optimization pathways through surface chemistry engineering and opens up new opportunities for the development of ultrasensitive sensors, with potential applicability in a broad range of fields and disciplines.

■ ASSOCIATED CONTENT

Supporting Information

The Supporting Information is available free of charge on the ACS Publications website at DOI: 10.1021/acsami.7b01116.

Synthesis process used to produce the cysteine-like compound AAC (PDF)

■ AUTHOR INFORMATION

Corresponding Authors

*(A.D.A.) Phone + 61 8 8313 5652; e-mail Andrew.abell@adelaide.edu.au.

*(A.S.) Phone +61 8 8313 1535; e-mail abel.santos@adelaide.edu.au.

ORCID

Dusan Losic: 0000-0002-1930-072X

Andrew D. Abell: 0000-0002-0604-2629

Abel Santos: 0000-0002-5081-5684

Notes

The authors declare no competing financial interest.

■ ACKNOWLEDGMENTS

Authors thank the support provided by the Australian Research Council (ARC) through the grants DE140100549, CE140100003, DP120101680, and FT110100711 and the School of Chemical Engineering (UoA). Authors thank the Adelaide Microscopy (AM) Centre for FEG-SEM characterization.

■ REFERENCES

(1) Fan, X.; White, I. M.; Shopova, S. I.; Zhu, H.; Suter, J. D.; Sun, Y. Sensitive Optical Biosensors for Unlabeled Targets: A review. *Anal. Chim. Acta* **2008**, *620*, 8−26.

(2) Jeffrey, W. C.; Daniel, M. R. Label-Free Biosensors for Biomedical Applications. In *Optical, Acoustic, Magnetic, and Mechanical Sensor Technologies*; CRC Press: 2012; pp 45−78.

(3) Gauglitz, G.; Moore, D. S. *Handbook of Spectroscopy*; John Wiley & Sons, Inc.: Weinheim, 2010.

(4) McDonagh, C.; Burke, C. S.; MacCraith, B. D. Optical Chemical Sensors. *Chem. Rev.* **2008**, *108*, 400−422.

(5) Borisov, S. M.; Wolfbeis, O. S. Optical Biosensors. *Chem. Rev.* **2008**, *108*, 423−461.

(6) Eggins, B. R. *Chemical Sensors and Biosensors*; John Wiley & Sons: West Sussex, 2008; Vol. *28*.

(7) Santos, A.; Kumeria, T.; Losic, D. Nanoporous Anodic Alumina: A Versatile Platform for Optical Biosensors. *Materials* **2014**, *7*, 4297−4320.

(8) Belge, G.; Beyerlein, D.; Betsch, C.; Eichhorn, K.-J.; Gauglitz, G.; Grundke, K.; Voit, B. Suitability of Hyperbranched Polyester for Sensoric Applications−Investigation with Reflectometric Interference Spectroscopy. *Anal. Bioanal. Chem.* **2002**, *374*, 403−411.

(9) Birkert, O.; Tünnemann, R.; Jung, G.; Gauglitz, G. Label-Free Parallel Screening of Combinatorial Triazine Libraries using Reflectometric Interference Spectroscopy. *Anal. Chem.* **2002**, *74*, 834−840.

(10) Gauglitz, G.; Brecht, A.; Kraus, G.; Mahm, W. Chemical and Biochemical Sensors Based on Interferometry at Thin (Multi-) Layers. *Sens. Actuators, B* **1993**, *11*, 21−27.

(11) Schmitt, H.-M.; Brecht, A.; Piehler, J.; Gauglitz, G. An Integrated System for Optical Biomolecular Interaction Analysis. *Biosens. Bioelectron.* **1997**, *12*, 809−816.

(12) Lin, V. S.-Y.; Motesharei, K.; Dancil, K.-P. S.; Sailor, M. J.; Ghadiri, M. R. A Porous Silicon-Based Optical Interferometric Biosensor. *Science* **1997**, *278*, 840−843.

(13) Dancil, K.-P. S.; Greiner, D. P.; Sailor, M. J. A Porous Silicon Optical Biosensor: Detection of Reversible Binding of IgG to a Protein A-Modified Surface. *J. Am. Chem. Soc.* **1999**, *121*, 7925−7930.

(14) Janshoff, A.; Dancil, K.-P. S.; Steinem, C.; Greiner, D. P.; Lin, V. S.-Y.; Gurtner, C.; Motesharei, K.; Sailor, M. J.; Ghadiri, M. R. Macroporous p-Type Silicon Fabry-Perot Layers. Fabrication, Characterization, and Applications in Biosensing. *J. Am. Chem. Soc.* **1998**, *120*, 12108−12116.

(15) Schwartz, M. P.; Alvarez, S. D.; Sailor, M. J. Porous SiO_2 Interferometric Biosensor for Quantitative Determination of Protein Interactions: Binding of Protein A to Immunoglobulins Derived from Different Species. *Anal. Chem.* **2007**, *79*, 327−334.

(16) Santos, A.; Balderrama, V. S.; Alba, M.; Formentín, P.; Ferré-Borrull, J.; Pallarès, J.; Marsal, L. F. Nanoporous Anodic Alumina Barcodes: Toward Smart Optical Biosensors. *Adv. Mater.* **2012**, *24*, 1050−1054.

(17) Salonen, J.; Laine, E.; Niinisto, L. Thermal Carbonization of Porous Silicon Surface by Acetylene. *J. Appl. Phys.* **2002**, *91*, 456−461.

(18) Chen, Y.; Santos, A.; Wang, Y.; Kumeria, T.; Wang, C.; Li, J.; Losic, D. Interferometric Nanoporous Anodic Alumina Photonic Coatings for Optical Sensing. *Nanoscale* **2015**, *7*, 7770−7779.

(19) Pan, S.; Rothberg, L. J. Interferometric Sensing of Biomolecular Binding using Nanoporous Aluminum Oxide Templates. *Nano Lett.* **2003**, *3*, 811−814.

(20) Alvarez, S. D.; Li, C.-P.; Chiang, C. E.; Schuller, I. K.; Sailor, M. J. A Label-Free Porous Alumina Interferometric Immunosensor. *ACS Nano* **2009**, *3*, 3301−3307.

(21) Kumeria, T.; Santos, A.; Losic, D. Ultrasensitive Nanoporous Interferometric Sensor for Label-Free Detection of Gold (III) Ions. *ACS Appl. Mater. Interfaces* **2013**, *5*, 11783−11790.

(22) Dronov, R.; Jane, A.; Shapter, J. G.; Hodges, A.; Voelcker, N. H. Nanoporous Alumina-Based Interferometric Transducers Ennobled. *Nanoscale* **2011**, *3*, 3109−3114.

DOI: 10.1021/acsami.7b01116
ACS Appl. Mater. Interfaces XXXX, XXX, XXX−XXX

(23) Nemati, M.; Santos, A.; Kumeria, T.; Losic, D. Label-Free Real-Time Quantification of Enzyme Levels by Interferometric Spectroscopy Combined with Gelatin-Modified Nanoporous Anodic Alumina Photonic Films. *Anal. Chem.* **2015**, *87*, 9016−9024.
(24) Law, C. S.; Santos, A.; Nemati, M.; Losic, D. Rational Engineering of Nanoporous Anodic Alumina Photonic Crystals by Sawtooth-Like Pulse Anodization. *ACS Appl. Mater. Interfaces* **2016**, *8*, 13542−13554.
(25) Santos, A.; Kumeria, T.; Losic, D. Optically Optimized Photoluminescent and Interferometric Biosensors Based on Nanoporous Anodic Alumina: A Comparison. *Anal. Chem.* **2013**, *85*, 7904−7911.
(26) Pacholski, C.; Sartor, M.; Sailor, M. J.; Cunin, F.; Miskelly, G. M. Biosensing Using Porous Silicon Double-Layer Interferometers: Reflective Interferometric Fourier Transform Spectroscopy. *J. Am. Chem. Soc.* **2005**, *127*, 11636−11645.
(27) Pacholski, C.; Yu, C.; Miskelly, G. M.; Godin, D.; Sailor, M. J. Reflective Interferometric Fourier Transform Spectroscopy: A Self-Compensating Label-Free Immunosensor Using Double-Layers of Porous SiO_2. *J. Am. Chem. Soc.* **2006**, *128*, 4250−4252.
(28) Masuda, H.; Fukuda, K. Ordered Metal Nanohole Arrays Made by a Two-Step Replication of Honeycomb Structures of Anodic Alumina. *Science* **1995**, *268*, 1466−1468.
(29) Masuda, H.; Yada, K.; Osaka, A. Self-Ordering of Cell Configuration of Anodic Porous Alumina with Large-Size Pores in Phosphoric Acid Solution. *Jpn. J. Appl. Phys.* **1998**, *37*, L1340−L1342.
(30) Masuda, H.; Hasegwa, F.; Ono, S. Self-Ordering of Cell Arrangement of Anodic Porous Alumina Formed in Sulfuric Acid Solution. *J. Electrochem. Soc.* **1997**, *144*, L127−L130.
(31) Nielsch, K.; Choi, J.; Schwirn, K.; Wehrspohn, R. B.; Gösele, U. Self-Ordering Regimes of Porous Alumina: The 10 Porosity Rule. *Nano Lett.* **2002**, *2*, 677−680.
(32) Santos, A.; Macías, G.; Ferré-Borrull, J.; Pallarès, J.; Marsal, L. F. Photoluminescent Enzymatic Sensor Based on Nanoporous Anodic Alumina. *ACS Appl. Mater. Interfaces* **2012**, *4*, 3584−3588.
(33) DeLouise, L. A.; Miller, B. L. Enzyme Immobilization in Porous Silicon: Quantitative Analysis of The Kinetic Parameters for Glutathione-S-Transferases. *Anal. Chem.* **2005**, *77*, 1950−1956.
(34) DeLouise, L. A.; Kou, P. M.; Miller, B. L. Cross-Correlation of Optical Microcavity Biosensor Response with Immobilized Enzyme Activity. Insights into Biosensor Sensitivity. *Anal. Chem.* **2005**, *77*, 3222−3230.
(35) Jani, A. M. M.; Kempson, I. M.; Losic, D.; Voelcker, N. H. Dressing in Layers: Layering Surface Functionalities in Nanoporous Aluminum Oxide Membranes. *Angew. Chem., Int. Ed.* **2010**, *49*, 7933−7937.
(36) Abràmoff, M. D.; Magalhães, P. J.; Ram, S. J. Image Processing with ImageJ. *Biophotonics Int.* **2004**, *11*, 36−42.
(37) Gunda, N. S. K.; Singh, M.; Norman, L.; Kaur, K.; Mitra, S. K. Optimization and Characterization of Biomolecule Immobilization on Silicon Substrates using (3-aminopropyl) triethoxysilane (APTES) and Glutaraldehyde Linker. *Appl. Surf. Sci.* **2014**, *305*, 522−530.
(38) Jadhav, S. A. Self-Assembled Monolayers (SAMs) of Carboxylic Acids: An Overview. *Cent. Eur. J. Chem.* **2011**, *9*, 369−378.
(39) Bandyopadhyay, K.; Patil, V.; Vijayamohanan, K.; Sastry, M. Adsorption of Silver Colloidal Particles through Covalent Linkage to Self-Assembled Monolayers. *Langmuir* **1997**, *13*, 5244−5248.
(40) Santos, A.; Kumeria, T.; Losic, D. Nanoporous Anodic Aluminum Oxide for Chemical Sensing and Biosensors. *TrAC, Trends Anal. Chem.* **2013**, *44*, 25−38.
(41) Anker, J. N.; Hall, W. P.; Lyandres, O.; Shah, N. C.; Zhao, J.; Van Duyne, R. P. Biosensing with Plasmonic Nanosensors. *Nat. Mater.* **2008**, *7*, 442−453.
(42) Mayer, K. M.; Hafner, J. H. Localized Surface Plasmon Resonance Sensors. *Chem. Rev.* **2011**, *111*, 3828−3857.
(43) Malinsky, M. D.; Kelly, K. L.; Schatz, G. C.; Van Duyne, R. P. Chain Length Dependence and Sensing Capabilities of the Localized Surface Plasmon Resonance of Silver Nanoparticles Chemically Modified with Alkanethiol Self-Assembled Monolayers. *J. Am. Chem. Soc.* **2001**, *123*, 1471−1482.
(44) Haes, A. J.; Zou, S.; Schatz, G. C.; Van Duyne, R. P. Nanoscale Optical Biosensor: Short Range Distance Dependence of The Localized Surface Plasmon Resonance of Noble Metal Nanoparticles. *J. Phys. Chem. B* **2004**, *108*, 6961−6968.

DOI: 10.1021/acsami.7b01116
ACS Appl. Mater. Interfaces XXXX, XXX, XXX−XXX